



Universal parameters and similarity conditions in the study of the diffracted signal around a wedge

Penelope Menounou¹, Marios Spiropoulos¹

¹Department of Mechanical Engineering and Aeronautics, University of Patras, Patras, Greece
(email: menounou@upatras.gr)

Abstract

A time domain model for predicting diffraction around rigid, infinitely long wedges is presented. An approximate solution is derived from the inverse Fourier transform of the frequency domain diffraction solutions provided by Oberhettinger. This solution unifies diffraction by plane, cylindrically and spherically spreading incident signals and provides a more rigorous extension of the Directive Line Source Model (DLSM) for diffraction around an arbitrary wedge. It is invalid for long times, wedge angles close to non-diffracting wedge angles and close to the shadow boundaries. The solution improves the accuracy of the original DLSM solution. It also provides significant insight into the mechanism of diffraction. Universal parameters are defined that describe similarities in the evolution of the diffracted signal around wedges of different angles. A generator curve is presented that embodies the diffracted signals for all source-wedge-receiver configurations. Finally, it is shown that the diffracted signal at any source-wedge-receiver configuration can be constructed from the diffracted signal at a uniquely identified source-receiver configuration around a half plane.

Keywords: wedge diffraction, time domain solution, generator curve, universal parameters

1 Introduction

The phenomenon of diffraction around wedges is important in acoustics, since it has many applications in areas such as oceanography, room acoustics, or noise barriers. It has been extensively studied, both theoretically/numerically and experimentally. The present work focuses on approximate analytical solutions in the time domain and its main purpose is to extend and enhance the Directive Line Source Model (DLSM) [1][2] to wedges of arbitrary angle. The derivation of the new approximate model starts with the frequency domain solutions for all three types of simple incident radiation (plane, cylindrical and spherical incident waves). The time domain solutions are derived by their frequency domain counterparts and appropriate approximations are introduced to derive the new solution (section 2). The new solution enhances the validity region of the original DLSM solution, while it maintains its simplicity. It is shown that universal parameters and the generator curve contemplated by the original DLSM for half planes can be extended to diffraction by a wedge for an arbitrary angle (section 3). Finally, it is shown that the new approximate solution allows us to correspond any source-wedge-receiver configuration of any wedge angle to a source-receiver configuration on the half plane (section 4).

The geometry of the problem and its main parameters is shown in Figure 1. A cylindrical coordinate system is considered with its z-axis on the diffracting edge of an infinitely long wedge. The angle of the wedge is 2Ω , and source and receiver can be located anywhere around the wedge. In wedge diffraction problems, the parameter γ is often used

$$\gamma = 2 \frac{(\pi - \Omega)}{\pi} \quad (1)$$

For $\gamma = 2/m$ and m an odd integer the diffracted signal at any location around the wedge becomes zero. Accordingly, the wedges are called *non-diffracting wedges* ($\Omega = 90^\circ, 135^\circ \dots$). For m an even integer, the diffracted field resembles that around a half plane and the wedges are called *neutral wedges* ($\Omega = 0^\circ, 120^\circ \dots$). The lines B^{I-II} and B^{II-III} shown in Figure 1(b) are called *shadow boundaries* and separate the diffracted field around the wedge into three regions, each one of which has a different number of geometrical acoustics contributions than its neighboring region.

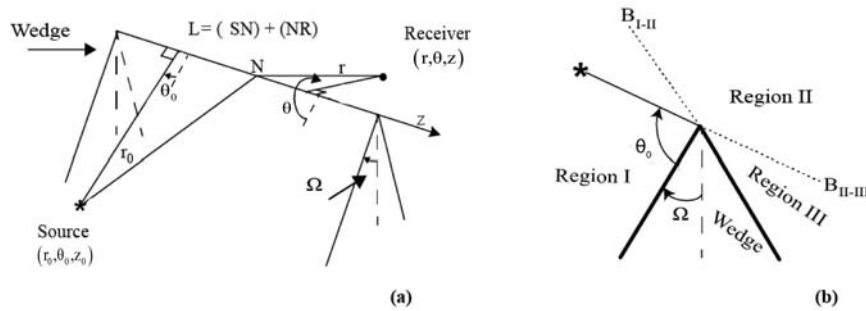


Figure 1: Geometry of the problem.

2 Wedge diffraction time domain solution

2.1 Unified representation of existing frequency domain solutions

For high frequencies $kr \gg 1$ (plane waves) or $kr r_0 / L \gg 1$ (cylindrical and spherical waves), the total acoustic field around a rigid wedge can be decomposed into a geometrical optics ($P^{g.o.}$) and a diffraction field (P^{diff}) component [3]

$$P = P^{g.o.} + P^{diff} \quad (2)$$

The diffracted component P^{diff} is the focus of the present work. Oberhettinger [4][5] presented the solution of the diffracted field for spherically and cylindrically spreading incident waves and for a plane wave incident on a rigid wedge. In the present work, it is proposed to consider the diffracted field caused by all types of incident radiation (plane waves, cylindrical and spherical incident waves) at a receiver in a unified representation as follows

$$P^{diff} = \frac{1}{2\pi\gamma} \int_0^\infty P_{spr} D d\zeta, \quad (3)$$

where $\zeta = \cosh^{-1}(F)$ is the equivalent angle between the source and receiver in the complex plane as defined in the literature with respect to Sommerfeld Contours [3], F varies with the type of the incident signal

$$F = \begin{cases} \frac{ct}{r}, & \text{plane} \\ \frac{c^2(t+r_0/c)^2 - r_0^2 - r^2}{2rr_0}, & \text{cylindrical} \\ \frac{c^2t^2 - r_0^2 - r^2 - (z-z_0)^2}{2rr_0}, & \text{spherical} \end{cases} \quad (4)$$

where c is the speed of sound, P_{spr} stands for a spreading term that depends on the type of the incident wave,

$$P_{\text{spr}} = \begin{cases} e^{ikrcosh(\zeta)}, & \text{plane} \\ H_0^{(1)}(kR(i\zeta)), & \text{cylindrical} \\ \frac{e^{ikR(i\zeta)}}{R(i\zeta)}, & \text{spherical} \end{cases}, \quad (5)$$

where $H_0^{(1)}$ is the Hankel function of the first kind, $R(i\zeta)$ is the equivalent distance between the source and the receiver in the complex plane

$$R(\zeta) = r^2 + r_0^2 - 2rr_0 \cos(i\zeta), \quad (6)$$

and D is a directivity function common for all types of incident radiation

$$D = \frac{\sin\left(\frac{\pi \pm \theta \pm \theta_0}{\gamma}\right)}{\cosh\left(\frac{\zeta}{\gamma}\right) - \cos\left(\frac{\pi \pm \theta \pm \theta_0}{\gamma}\right)}, \quad (7)$$

where $(\pi \pm \theta \pm \theta_0)/\gamma$ represents the summation of four terms.

2.2 Exact time domain solutions

In this subsection the impulse response solution is obtained by calculating the inverse Fourier transform of the frequency domain solution [Eq. (3)] [6]. The following variable change is employed

$$d\zeta = \frac{1}{\sinh(\zeta)} \frac{dF}{dt}, \quad (8)$$

while combination of Eqs. (4) and (6) yields that $R(i\zeta) = ct$. For cylindrically spreading incident waves the asymptotic forms for the Hankel function $H_0^{(1)}(kR) = \sqrt{2/kR\pi} e^{ikR - i\pi/4}$ for $kR \gg 1$ is used. The impulse response solution obtained by the inverse Fourier transform is

$$p^{\text{irf}} = p_{\text{amp}} p_{\text{spr}} D, \quad (9)$$

where p_{amp} is an amplitude factor and p_{spr} shows the time evolution of the diffracted signal around the wedge. The terms p_{amp} and p_{spr} depend on the type of incident signal, while the directivity function D is the same as its frequency domain counterpart.

$$p_{\text{amp}} = \begin{cases} -\frac{c}{2\gamma\pi r}, & \text{plane} \\ -\frac{c}{2\gamma\pi r} \frac{1}{\sqrt{r_0}} \frac{H(t-r_0/c)}{\sqrt{t^2-r_0^2/c^2}}, & \text{cylindrical} \\ -\frac{c}{2\gamma\pi r r_0}, & \text{spherical} \end{cases} \quad (10)$$

$$p_{\text{spr}} = \begin{cases} \frac{1}{\sinh(\zeta)}, & \text{plane, spherical} \\ -\frac{c}{2\gamma\pi r} \frac{1}{\sqrt{r_0}} \frac{H(t-r_0/c)}{\sqrt{t^2-r_0^2/c^2}} * H(t-r/c) \frac{\sqrt{t+r_0/c}}{\sinh(\zeta)}, & \text{cylindrical} \end{cases} \quad (11)$$

For spherically spreading signals Equation (9) is identical to the exact Biot-Tolstoy solution [7], which in the following will be referred to as BTMS from the names of its main contributors (Biot-Tolstoy-Medwin-Svensson [8]). For plane incident signals Equation (9), after some algebraic manipulations, it can be transformed to the exact time domain solution proposed by Friedlander [9]. The impulse response for cylindrically spreading incident signals is approximate (recall the employment of the asymptotic form of the Hankel function in the derivation).

2.3 Approximate time domain solutions

In this section a new approximate time domain solution is derived. The main advantage of this newly presented solution is that it maintains the same simple form of the Directive Line Source Model [1], [2], while it extends its region of validity, since it comes from the exact time domain solutions of Eqs. (9) - (11). Firstly, we assume times shortly after the arrival of the diffracted signal, that is $t \rightarrow L/c$ or equivalently $F \rightarrow 1$. As a result, using the properties of the hyperbolic trigonometric functions, we obtain $\sinh(\zeta) = \sqrt{F+1}\sqrt{F-1} \approx \sqrt{2}\sqrt{F-1}$. Furthermore, the assumption of short times allows us to use the Taylor expansions of hyperbolic trigonometric functions

$$\begin{aligned} \sinh(\zeta) &\approx \zeta \approx \sqrt{2}\sqrt{F-1} \\ \cosh(\zeta/\gamma) &\approx 1 + \frac{1}{2} \left(\frac{\zeta}{\gamma} \right)^2 \approx 1 + \frac{1}{2} \left(\frac{\sqrt{2}\sqrt{F-1}}{\gamma} \right)^2. \end{aligned} \quad (12)$$

Substituting Equations (12) into (9) and after some algebraic manipulation the approximate time domain model can be described by two terms (instead of four). In the second step of the derivation, it is assumed that $\tau = t - t_d \ll \bar{t}\gamma^2$ and $O(\tau^2) \approx 0$, where $O(\tau)$ corresponds to the order of magnitude of τ and t_d is defined in Eq. (18). The new approximate solution termed modified Directive Line Source Mode (mDLSM) is the following

$$p^{\text{irf}} = -\frac{1}{4\pi} A_t * (I_d d), \quad (13)$$

where $*$ is the convolution sign, A_t an amplitude parameter that depends on the incident radiation

$$A_t = \begin{cases} 1, & \text{plane} \\ H\left(t - \frac{r_0}{c}\right) \frac{1}{\sqrt{t^2 - \frac{r_0^2}{c^2}}}, & \text{cylindrical} \\ \frac{1}{\sqrt{rr_0}}, & \text{spherical} \end{cases} \quad (14)$$

I_d represents the time evolution of the signal that is equivalent to radiation from a line source

$$I_d = \frac{2}{\sqrt{t^2 - t_d^2}} \quad (15)$$

and d represents a new directivity function

$$d = d^i + d^r, \quad d^{ir} = \sqrt{2\gamma t} \sqrt{\frac{t}{t_d} + 1} \frac{\bar{\Phi}_{i,r}}{2(t-t_d) \left(\bar{\gamma}^2 - \cot\left(\frac{\pi}{\gamma}\right) \bar{\Phi}_{i,r} \right) + \bar{\Phi}_{i,r}^2}, \quad (16)$$

where $\bar{\Phi}_{i,r}$ is a parameter mainly dependent on the wedge angle and the angular location of the source and the receiver.

$$\bar{\Phi}_{i,r} = \gamma^2 \bar{t} \frac{\cos\left(\frac{\theta \pm \theta_0}{\gamma}\right) - \cos\left(\frac{\pi}{\gamma}\right)}{\sin\left(\frac{\pi}{\gamma}\right)}. \quad (17)$$

Moreover, the following time parameters are introduced

$$t_d = \begin{cases} \frac{r}{c}, & \text{plane \& cylindrical} \\ \frac{L}{c}, & \text{spherical} \end{cases} \quad (18)$$

where t_d is the time that the signal needs to travel from the edge to the receiver and \bar{t}

$$\bar{t} = \begin{cases} \frac{r}{c}, & \text{plane} \\ \frac{rr_0}{Lc}, & \text{cylindrical \& spherical} \end{cases} \quad (19)$$

is another time parameter that if multiplied with the angular frequency ω , it yields the criterion for separating the acoustic field into a geometrical and a diffraction component (i.e. for spherical incident radiation $\omega \bar{t} = krr_0 / L \gg 1$). The new approximate solution [Eq. (13)] shares the same mathematical simplicity with

the Directive Line Source Model in the time domain [2]. Their main difference lies in their different directivity functions [Eq. (16)]. Both solutions have two terms

$$p^{\text{irf}} = p^{\text{irf},i} + p^{\text{irf},r}, \quad (20)$$

where $p^{\text{irf},i}$ will be called for simplicity *incident term* and is associated to the directivity term d^i and the *incident parameter* $u = (\theta - \theta_0)/\gamma$ and $p^{\text{irf},r}$ will be called *reflected term* and is associated to d^r and the reflected parameter $v = (\theta + \theta_0)/\gamma$.

2.4 Accuracy of the new approximate time domain solution

The accuracy of the proposed solution is investigated by numerically comparing results obtained by the new approximate solution (mDLSM), the original DLSM solution (DLSM) and the exact time domain solution (BTMS). The comparison is done for spherically spreading incident signals. The comparison results are presented in Figure 3. The relative error of the approximate models (mDLSM in Fig. 2(a)(b) and DLSM in Fig. 2(c)(d)] with the exact BTMS solution is presented for all combinations of wedge angles Ω and all source-receiver angular locations θ, θ_0 in a single plot. The combination of all θ, θ_0 is done via use of the incident and reflected parameters u and v . The relative error of each term of the approximate solutions ($p^{\text{irf},i}$ associated with u and $p^{\text{irf},r}$ associated with v) is considered separately and compared against the corresponding term of the exact BTMS solution (in the form given by Pierce as a solution of two instead of four terms [10].) The red lines in Fig. 2 correspond to the shadow boundaries. As Ω increases (over 160°) the shadow boundaries come closer and closer until they collapse at $\Omega = 180^\circ$. The black-colored area shows combinations of parameters that yield relative error over 10%. This happens close to the shadow boundaries and for wedge angles close to the non-diffracting wedges. The comparisons are shown for a given time $\tau^* = (t^* - t_d) = 0.025(\bar{t}\gamma^2)$. At longer times the black-colored areas expand, at shorter times the areas shrink. The time τ^* is based on the assumptions made for the derivation of the solution. Finally, in almost all cases, the presented mDLSM solution improves the accuracy of the original DLSM solution.

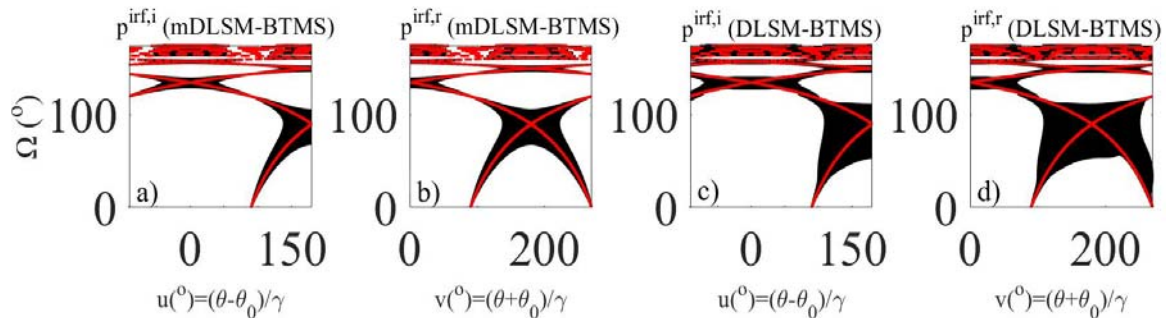


Figure 2: Contours of relative error with the exact BTMS solution of the mDLSM [(a)(b)] and of the DLSM solution [(c)(d)] at time $\tau^* = 0.025(\bar{t}\gamma^2)$. The terms $p^{\text{irf},i}$ and $p^{\text{irf},r}$ in the mDLSM and the DLSM are compared separately against the corresponding terms of the BTMS solution.

3 Universal Parameters-Similarity Conditions

Within its region of validity, the presented time domain solution allows us to define a generator curve- a single curve that generates all diffracted signals for all source receiver locations, all types of incident radiation and all wedge angles. The concept of the generator curve has been introduced in [2] for half planes

and it is shown here that it can be extended to wedges of arbitrary angle. Extending the analysis in [2] we redefine the two diffraction numbers

$$\Pi^{i,r} = \frac{\tau}{\tau_{\text{lag}}^{i,r}}, \quad (21)$$

where $\tau = t - t_d$ is the *diffraction time* (i.e. the time that starts when the diffracted signal arrives at the receiver) and $\tau_{\text{lag}}^{i,r}$ are the *diffraction delay times* defined as

$$\tau_{\text{lag}}^{i,r} = \frac{\overline{\Phi}_{i,r}^2}{2 \left(\overline{t\gamma}^2 - \cot \left(\frac{\pi}{\gamma} \right) \overline{\Phi}_{i,r} \right)}. \quad (22)$$

$$\tau_{\text{lag}}^{i,r} = \frac{\overline{\Phi}_{i,r}^2}{2 \left(\overline{t\gamma}^2 - \cot \left(\frac{\pi}{\gamma} \right) \overline{\Phi}_{i,r} \right)}. \quad (23)$$

The diffraction number Π is a dimensionless number that normalizes τ with the diffraction delay time, which in turn is determined by the specific source-wedge-receiver configuration. The diffraction delay times describe proximity to the shadow boundaries. Figure (3) shows the contours of $\tau_{\text{lag}}^{i,r}$ along with the shadow boundaries (red lines) for all wedge angles Ω and all source-receiver configurations. It can be observed that both τ_{lag}^i and τ_{lag}^r become zero at the shadow boundaries. It can also be observed that different source-wedge-receiver configurations have the same diffraction delay time. The later observation allows to determine angular similarities between wedges, as will be shown in section 4.

Figure 3(c) shows that at a location with large diffraction delay time τ_{lag}^i (i.e. away from the shadow boundary) the corresponding impulse response $p^{\text{irf},i}$ evolves slower with time. At locations with small diffraction delay times (close to the shadow boundaries), most of the acoustics energy is released at short diffraction times and $p^{\text{irf},i}$ evolves faster with time.

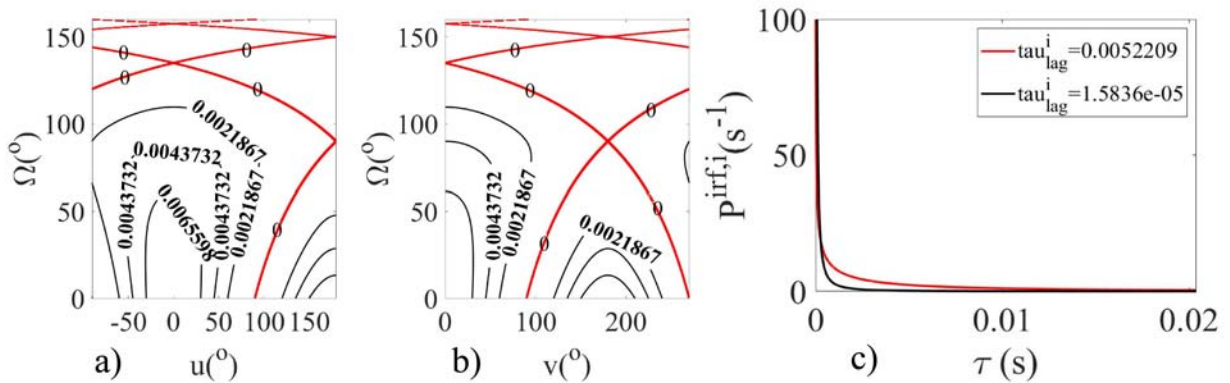


Figure 3: Diffraction delay times τ_{lag}^i (a), τ_{lag}^r (b) for different wedge angles τ and source-receiver combinations; impulse responses $p^{\text{irf},i}$ at locations with different τ_{lag}^i (c).

3.1 Generator curve

As it was shown in ref. [2] any impulse response solution around a half plane can be incorporated into a single curve, called the *generator curve* which depends solely on the diffraction number Π . In order to obtain the impulse response signal from the generator curve, one should scale it with an appropriate scaling function. It can be shown that the notion of the generator curve and the scaling function can be extended for any arbitrary wedge as follows

$$E^{i,r} = \frac{4\sqrt{2}}{\pi\sqrt{\pi}\sqrt{\Pi^{i,r}}(\Pi^{i,r}+1)} \quad (24)$$

$$S^{i,r} = -\frac{\gamma\sqrt{\pi}}{8} \frac{\bar{t}}{\sqrt{t_d}\tau_{lag}^{i,r}\Phi_{1/2}} A_t, \quad (25)$$

where $E^{i,r}$ corresponds to the generator curve and is the same for all types of incident signals, while the scaling factor $S^{i,r}$ depends on the geometry of the specific source-receiver configuration. It is noted that the generator curve is the same as in the case of the half plane, while the scaling factor differs. Any impulse response regardless of the type of incident signal can be generated as follows

$$p^{irf} = p^{irf,i} + p^{irf,r} = S^i * E^i + S^r * E^r \quad (26)$$

Figure 4 depicts the generator curve for the incident term E^i [(a)]. From the generator curve all impulse responses $p^{irf,i}$ can be derived. Figure 4 shows so generated impulse responses (solid line) for plane [(b)], spherical [(c)] and cylindrical [(d)] incident signals for different source-wedge-receiver configurations. The impulse responses obtained directly by the analytical solution (dashed line) are the same as the impulse responses derived by the generator curve.

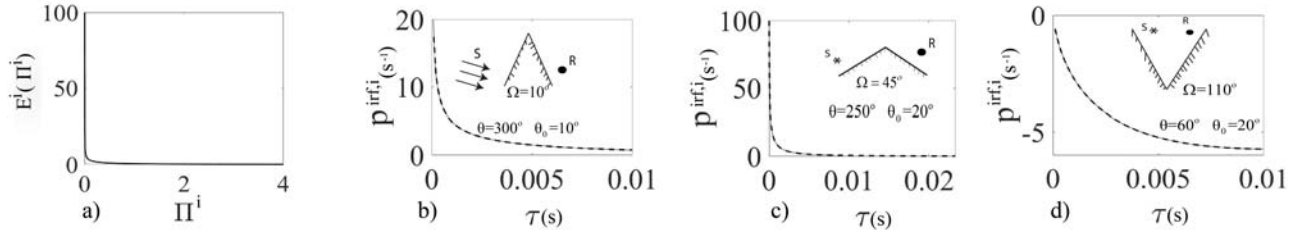


Figure 4: The generator curve E^i depends only on the dimensionless diffraction number Π^i [(a)]. The impulse response for plane [(b)], spherical [(c)], and cylindrical [(d)] incident signals around various wedge angles and for various source-receiver locations. The impulse responses obtained directly by the analytical solution (dashed line) are the same as the impulse responses derived by the generator curve (solid line).

4 Mapping of all wedges into a half plane

Within its region of validity, the presented diffraction solution allows us to map any source-wedge-receiver configuration to a uniquely identified source-receiver configuration around a half plane. The correspondence can be important as the diffracted field around a half plane has been extensively studied (both theoretically and experimentally); more than the diffracted field around arbitrary wedges (particularly closed wedges). Consider an arbitrary source-wedge-receiver configuration. For constant radial and z-coordinates of source and receiver the following angular mapping is introduced

$$p_w^{irf} = W^i \Big|_{hp \rightarrow w} p_{hp}^{irf,i} + W^r \Big|_{hp \rightarrow w} p_{hp}^{irf,r}, \quad (27)$$

where $W_{hp \rightarrow w}^{i,r}$ is called the *wedge factor* and is the ratio of the directivity functions of the wedge and of the half plane

$$W_{hp \rightarrow w}^{i,r} = \frac{d_w^{i,r}}{d_{hp}^{i,r}} = \frac{\gamma_w}{2} \frac{\overline{\Phi}_{hp}^{i,r} (\Pi_{hp}^{i,r} + 1) \Pi_w^{i,r}}{\overline{\Phi}_w^{i,r} (\Pi_w^{i,r} + 1) \Pi_{hp}^{i,r}}. \quad (28)$$

Equations (28) and (29) can be simplified, provided that $\Pi_w^{i,r} = \Pi_{hp}^{i,r}$. In such case, the wedge factor becomes

$$W_{hp \rightarrow w}^{i,r} = \frac{\gamma_w}{2} \frac{\overline{\Phi}_{hp}^{i,r}}{\overline{\Phi}_w^{i,r}}. \quad (29)$$

The wedge factor has no time dependence and therefore Eq. (28) can be employed not only for the impulse response but for the diffracted signal caused by any arbitrary incident signal, as well. (The diffracted signal is obtained by convolving the impulse response with the incident signal. The time-independent wedge factor does not affect the convolution integral). The equality of two different diffraction numbers $\Pi_w^i = \Pi_{hp}^i$ and $\Pi_w^r = \Pi_{hp}^r$ holds for any τ , provided that $\tau_{lag,w}^i = \tau_{lag,hp}^i$ and $\tau_{lag,w}^r = \tau_{lag,hp}^r$. This results into the following equations

$$\begin{cases} \overline{\Phi}_{i,w}^2 - 8\tau_{lag}^i = 0 \\ \overline{\Phi}_{r,w_2}^2 - 8\tau_{lag}^r = 0 \end{cases}. \quad (29)$$

Equations (30) have one double solution each and therefore an arbitrary source-wedge-receiver configuration can be mapped (corresponded) into a source-receiver configuration around a half plane. An example is shown in Fig. (5). Consider a wedge $\Omega=45^\circ$ and $\theta=220^\circ, \theta_0=10^\circ$. Solving for the angular locations in Eq. (30) the corresponding source and receiver locations around a half plane are $\theta^*=218.10^\circ, \theta_0^*=8.67^\circ$. The impulse response around the wedge obtained directly by mDLSM for the wedge (solid line) is identical to the impulse response obtained by the corresponding configuration around the half plane [via Eq. (28)] (dashed line). The same holds for an N-wave response.

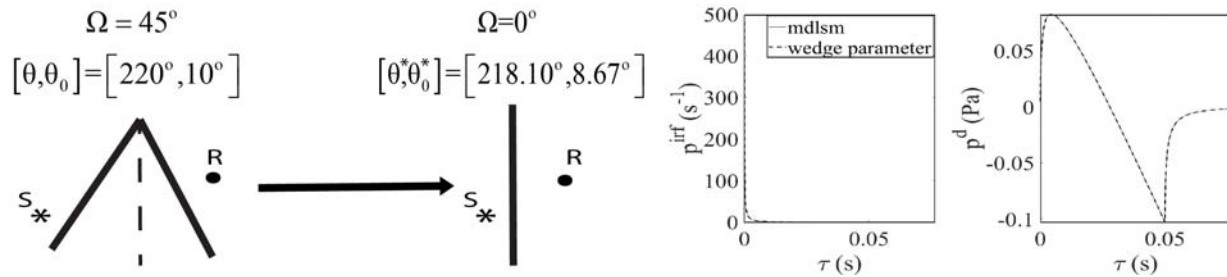


Figure 5: The impulse response and the N-wave response for the wedge configuration shown on the left is identical to the impulse response and the N-wave response constructed via Eq. (28) from the impulse response for the half plane configuration shown in the middle.

For different wedge angles the ranges of the corresponding source and receiver locations around the half plane θ^*, θ_0^* differ. Figure 6 shows the ranges of the source and receiver location in the half plane θ^*, θ_0^* that correspond to all source and receiver combinations around two wedges. It can be observed that the mapping regions (hatched areas) around the half plane shrink as the wedge angle increases.

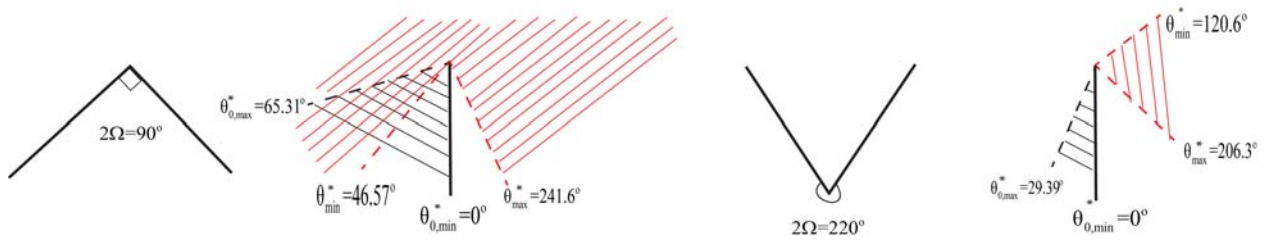


Figure 6: Ranges of source and receiver locations around the half plane θ^* , θ_0^* that correspond to all source and receiver combinations around a wedge of $\Omega=45^\circ$ and of $\Omega=110^\circ$.

5 Conclusions

A new approximate time domain solution is presented that describes the diffracted signal around a rigid wedge of arbitrary angle. The solution is valid for short diffraction times, away from the shadow boundaries and for wedges angles that are not very close to non-diffracting wedges. The new solution allows the definition of universal parameters that describe the time evolution of the diffracted signal and of a generator curves that embodies all diffracted signals for all source-wedge-receiver configuration. Finally, it is shown that the diffracted signal at any source-wedge-receiver configuration can be constructed from the diffracted signal at a uniquely identified source-receiver configuration around a half plane.

References

- [1] Menounou, P. and Nikolaou, P., 2016. An Extension to the Directive Line Source Model for Diffraction by Half Planes and Wedges. *Acta Acustica united with Acustica*, 102(2), pp.307-321.
- [2] Menounou, P. and Nikolaou, P., 2017. Analytical model for predicting edge diffraction in the time domain. *Journal of the Acoustical Society of America*, 142(6), pp.3580-3592.
- [3] J. J. Bowman and T. B. A. Senior, *Electromagnetic and Acoustic Scattering by Simple Shapes*, edited by J. J. Bowman, T. B. A. Senior, and P. L. E. Uslenghi. North-Holland, Amsterdam, 1969.
- [4] Oberhettinger, F., 1954. Diffraction of waves by a wedge. *Communications on Pure and Applied Mathematics*, 7(3), pp.551-563.
- [5] Oberhettinger, F., 1955. On Asymptotic Series for Functions Occurring in the Theory of Diffraction of Waves by Wedges. *Journal of Mathematics and Physics*, 34(1-4), pp.245-255.
- [6] Nikolaou, P., personal communication
- [7] Biot, M. A. and Tolstoy, I. Formulation of Wave Propagation in Infinite Media by Normal Coordinates with an Application to Diffraction. *Journal of Acoustical Society of America*, pp.381-391.
- [8] Svensson, U.P, Fred, R.I., and Vanderkooy J. 1999. An analytic secondary source model of edge diffraction impulse responses. *Journal of the Acoustical Society of America*, 106(6), pp.2331-2334.
- [9] F.G. Friedlander, The diffraction of sound pulses II. Diffraction by an infinite wedge, Proceedings of the Royal Society of London. Series A, Mathematical and Physical Sciences, Vol. 186, No. 1006 (Sep. 24, 1946), pp. 322-3.
- [10] Pierce AD. *ACOUSTICS. An introduction to its physical principles and applications*. Acoustical Society of America, New York (USA), 1989.